NACA

RESEARCH MEMORANDUM

EXTERNAL-STREAM EFFECTS ON GROSS THRUST AND PUMPING CHARACTERISTICS OF EJECTORS OPERATING AT OFF-DESIGN MACH NUMBERS

By Alfred S. Valerino and Richard A. Yeager

Lewis Flight Propulsion Laboratory
Cleveland, Ohio

NATIONAL ADVISORY COMMITTEE
FOR AERONAUTICS

WASHINGTON
June 26, 1956

NATIONAL ADVISORY COMMITTEE FOR AERONAUTICS

RESEARCH MEMORANDUM

EXTERNAL-STREAM EFFECTS ON GROSS THRUST AND PUMPING CHARACTERISTICS OF EJECTORS OPERATING AT OFF-DESIGN MACH NUMBERS

By Alfred S. Valerino and Richard A. Yeager

SUMMARY

An investigation was conducted in the NACA Lewis 8- by 6-foot supersonic tunnel to determine the external-stream effects on the gross thrust and pumping characteristics of ejectors operating at off-design Mach numbers. Ejectors having diameter ratios of 1.16, 1.45, and 1.70 were tested over a range of primary-jet pressure ratios and secondary weight flows at free-stream Mach numbers of 0, 0.63, 1.5, 1.8, and 2.0. Design Mach numbers of the 1.16-, 1.45-, and 1.70-diameter-ratio ejectors, obtained by assuming an inlet total-pressure recovery on a current-production engine, were approximately 1.7, 2.2, and 2.6, respectively. The spacing ratio of the 1.70-diameter-ratio ejector was varied from 0 to 1.19.

Results of the investigation indicate that the primary-jet pressure ratio above which quiescent-air and supersonic-air data agree decreased with decreasing diameter ratio and with increasing spacing ratio. Increases in secondary weight flow reduced the primary-jet pressure ratio above which external-stream effects disappear. No external-stream effects were found at a free-stream Mach number of 0.63. Quiescent-air data overestimated the gross jet thrust of high-diameter-ratio ejectors operating below design conditions with low values of secondary weight flow. External-stream effects on ejector gross-jet-thrust ratios resulted from low base pressures obtained at supersonic speeds.

INTRODUCTION

In order to fully evaluate an exhaust system for supersonic aircraft, the interaction effects between the jet and the external stream must be known. The jet can affect the flow over the afterbody, thereby altering the drag. In addition, the external stream can alter the internal-flow characteristics and under some conditions affect the thrust.

Recent ejector-nozzle data (ref. 1), obtained in the NACA Lewis 8- by 6-foot supersonic tunnel, indicate that at design conditions the jet thrust and pumping characteristics agree with quiescent-air data. At jet pressure ratios below design, however, the reduced pressures in the base region cause the jet to overexpand (ref. 2) with the result that both thrust and pumping characteristics do not agree with data obtained in quiescent air.

In order to extend the available data on the effects of external stream on the performance of ejector nozzles operating at off-design conditions, an investigation was conducted in the NACA Lewis 8- by 6-foot supersonic tunnel. Ejectors having diameter ratios of 1.16, 1.45, and 1.70 were tested with variable secondary flow at zero angle of attack and at free-stream Mach numbers of 0, 0.63, 1.5, 1.8, and 2.0. Spacing ratios of the 1.16- and 1.45-diameter-ratio ejectors were 0.38 and 0.48, respectively. The spacing ratio of the 1.70-diameter-ratio ejector was varied from 0 to 1.19. By assuming an inlet total-pressure recovery on a current-production engine, design Mach numbers of the 1.16-, 1.45-, and 1.70-diameter-ratio ejectors of approximately 1.70, 2.2, and 2.6, respectively, were calculated. The 1.70- and 1.45-diameter-ratio ejectors serve as nonafterburning configurations throughout the Mach number range investigated. The temperature of the exhaust jet was maintained at approximately 760° R.

SYMBOLS

The following symbols are used in this report:

A	area, sq ft
C_D	drag coefficient based on maximum frontal area
C_p	pressure coefficient, $(p - p_0)/q_0$
D_p	primary-nozzle-exit diameter, in.
D_s	shroud-exit diameter, in.
D_p/D_s	diameter ratio
F	gross jet thrust, lb
M	Mach number
P	total pressure, lb/sq ft
p	static pressure, lb/sq ft

q	dynamic pressure, lb/sq ft
r	radius, in.
S	distance from primary-nozzle exit to shroud exit, in.
S/D_p	spacing ratio
T	total temperature, $^{\circ}R$
w	weight flow, lb/sec
$\frac{w_s}{w_p}\sqrt{\frac{T_s}{T_p}}$	corrected weight-flow ratio
x	distance along afterbody, in.

Subscripts:

a	boattail
b	shroud base
e	ejector
i	conditions above which stream effects are eliminated
p	primary
s	secondary
0	free stream

APPARATUS AND PROCEDURE

Model Installation

The jet exit model was installed in the Lewis 8- by 6-foot supersonic tunnel as shown in figure 1. Internal flow was obtained from a separately controlled air supply. The air, preheated to 300° F, was introduced into the model by means of the two hollow support struts. A more detailed discussion of the tunnel installation can be found in reference 3.

The quiescent-air test rig was located in the lower balance chamber of the 8- by 6-foot supersonic tunnel. The range of primary-nozzle jet pressure ratios was obtained by introducing high-pressure air into the

model and varying the ambient pressure of the balance chamber by means of an exhauster system.

A schematic diagram of the model showing internal details and pertinent external model stations is presented in figure 2. Air for the ejector secondary passage was obtained from the primary-air supply by means of a controlled calibrated bleed valve. Also shown in figure 2 are components of the model connected to the strain-gage balance.

Ejector Configurations

The ejector configurations investigated were obtained by using three primary-jet nozzles in conjunction with a fixed afterbody. Coordinates of the fixed-afterbody section are shown in figure 3. The contour of the afterbody was parabolic for the first 10 inches of its length and then conical for the next 6.93 inches. The conical section was followed by a parabolic shroud. Internal diameters of the entrance and exit stations of the afterbody were 8.0 and 4.34 inches, respectively. The shroud exit angle was 24.5°.

Schematic diagrams of the three primary-jet nozzles are presented in figure 4. Nozzles A and B were conical nozzles with exit diameters of 3.74 and 3.00 inches, respectively. Nozzle C was a contoured nozzle with an exit diameter of 2.55 inches. The entrance diameter of each nozzle was 4.10 inches. Calibrated flow discharge coefficients of 0.99, 0.98, and 1.0 were obtained for nozzles A, B, and C, respectively. The design Mach numbers obtained by assuming an inlet total-pressure recovery on a current-production engine, and the diameter ratios D_s/D_p obtained by using the three nozzles with the fixed afterbody, are shown in the following table:

Design Mach number, M	Nozzle	D_s/D_p
1.7	A	1.16
2.2	B	1.45
2.6	C	1.70

Spacing ratios S/D_p of 0, 0.38, 0.48, 0.56, 0.85, and 1.19 were obtained by inserting constant-area sections of various lengths upstream of the afterbody at model station 49.25.

Schematic diagrams of the ejector configurations investigated are presented in figure 5. Each configuration is designated by two numbers;

the first number refers to the diameter ratio and the second to the spacing ratio. Configurations 1.16-0.38 and 1.45-0.48 consisted of the fixed afterbody with nozzles A and B, respectively, and with a spacer of 1.44 inches inserted upstream of the afterbody at model station 49.25. Configurations 1.70-0, 1.70-0.56, 1.70-0.85, and 1.70-1.19 consisted of the afterbody with nozzle C and spacer lengths of 0, 1.44, 2.19, and 3.0 inches, respectively.

Data Reduction

Total weight flow through the model was determined from the sharp-edged orifice shown in figure 1 and a rotameter, which measured the preheater fuel flow. The primary-nozzle weight flow w_p was obtained by subtracting the weight flow through the calibrated bleed valve w_s from the total weight flow. The total temperature was measured in the support struts and was assumed constant throughout the model. The primary-nozzle total pressure P_p was calculated from continuity relations at the nozzle entrance, where the area, static pressure, weight flow, and temperature were known. The secondary total pressure P_s was obtained from a total-pressure rake located in the secondary passage.

The base pressures were measured with four static orifices located in the base of the shroud, as shown in figure 3. Boattail drags were found by integrating the boattail static pressures (fig. 3).

The method of force measurement and the reduction of these data are described in detail in reference 1. The gross ejector thrust is equal to the thrust-minus-drag (measured by the strain-gage balance) plus the summation of forebody and afterbody drag (obtained from jet-off reading and boattail drag).

RESULTS AND DISCUSSION

Pumping, Thrust, and Base Pressure Characteristics

Flow conditions at the exit plane of any nozzle depend on the pressure ratio P_p/p_b, where p_b is the local pressure on the base just downstream of the exit. However, test-stand performance data are presented as a function of the pressure ratio P_p/p_0, since the local pressure p_b is equal to ambient pressure. In supersonic flight, the nozzle performance, when expressed as a function of the pressure ratio P_p/p_0 $\left(\text{where } \frac{P_p}{p_0} = \frac{P_p}{p_b}\frac{p_b}{p_0}\right)$, will differ from the test-stand performance if the ratio p_b/p_0 is not equal to unity. However, for any nozzle there does

exist a pressure ratio $(P_p/p_b)_i$ above which the nozzle-exit Mach number and the ratio of the exit static pressure to nozzle total pressure are invariant with pressure ratio. This pressure ratio is dependent upon nozzle geometry and is the pressure ratio at which the flow is fully expanded. There is also another pressure ratio $(P_p/p_0)_i$ above which exit flow conditions are independent of stream effects. This value is given by

$$\left(\frac{P_p}{p_0}\right)_i = \left(\frac{P_p}{p_b}\right)_i \left(\frac{p_b}{p_0}\right)_{max}$$

4026

where $(p_b/p_0)_{max}$ is the maximum value which will occur over the flight speed range of interest. It should be noted that the pressure ratio $(P_p/p_0)_i$ depends on afterbody shape and flight speed range as well as nozzle geometry.

For an ejector nozzle, the geometry and therefore the pressure ratio $(P_p/p_0)_i$ are determined by the diameter ratio, shroud length, and secondary-to-primary weight-flow ratio. This is illustrated in the ejector performance characteristics presented in figures 6 to 11. A comparison of the performances of ejectors 1.16-0.38, 1.45-0.48, and 1.70-0.56 (figs. 6, 7, and 9, respectively) indicate that, the lower the ejector diameter ratio, the lower the primary-jet pressure ratio $(P_p/p_0)_i$ above which quiescent-air and supersonic-air data agree. In figure 6, it is assumed that quiescent-air and supersonic-air data agree since no effects were found with variable supersonic Mach numbers. Increasing the ejector diameter ratio results in thrust losses (due both to the overexpansion of the primary jet and to the adverse external-stream effects) when flight Mach number is changed from 0 to a supersonic value. The overexpansion of the primary jet and the adverse stream effects result from low base pressures obtained at supersonic flight speeds.

A comparison of the performances of configurations 1.70-0, 1.70-0.56, 1.70-0.85, and 1.70-1.19 (figs. 8, 9, 10, and 11, respectively) indicate that, the higher the spacing ratio, the lower the primary pressure ratio $(P_p/p_0)_i$ above which quiescent-air and supersonic-air data agree. This results since increasing the ejector spacing ratio lowers the primary-jet pressure ratio P_p/p_0 required to choke the secondary-flow passage. Since configuration 1.70-0 (fig. 8) has zero shroud length, external-stream effects are apparent at all pressure ratios, that is, $(P_p/p_0)_i \to \infty$.

For all configurations tested, increasing secondary flow decreases the value of primary-jet pressure ratio $(P_p/p_0)_i$ above which quiescent-air and supersonic-air data agree. Therefore, increasing secondary weight flow reduces the external-stream effects.

Subsonic data ($M_0 = 0.63$) agree with quiescent-air data, regardless of configuration. Obviously, at a Mach number of 0.63, the pressure ratio p_b/p_0 must be close to unity.

As mentioned earlier in this section, the flow conditions at the exit should depend on the pressure ratio P_p/p_b. Therefore, the ejector secondary-to-primary total-pressure ratio P_s/P_p and the exit momentum should depend only on the pressure ratio P_p/p_b. Gross thrust will depend on both P_p/p_b and P_p/p_0, because it includes a pressure-area term p_0A_s. Exit momenta for the ejectors were not computed, but the ejector secondary-to-primary total-pressure ratio P_s/P_p is presented as a function of the pressure ratio P_p/p_b in figure 12. By maintaining the same primary-jet total- to base-static-pressure ratio P_p/p_b, the same pumping characteristics will be obtained, regardless of flight speed.

4026

Boattail Drag Characteristics

Typical jet effects on afterbody pressure distribution are presented in figure 13. As the base pressure is increased, due to changes in nozzles and jet pressure ratios, the rearmost boattail pressure coefficients $C_{p,a}$ also increase.

Since the same afterbody was used in conjunction with the three primary-jet exhaust nozzles, it should be possible to generalize results for all configurations by plotting the drag coefficient of all configurations investigated against the ratio of base-to-free-stream static pressure p_b/p_0. The boattail drag characteristics are shown in figure 14. Because of the increase in boattail pressure coefficient with increasing base pressure, the boattail drag coefficient decreases with increasing base-to-free-stream static-pressure ratio. Increasing the supersonic free-stream Mach number results in a slight decrease in boattail drag coefficient.

The ejector gross-jet-thrust ratio F_e/F_p as well as the secondary-to-primary total-pressure ratio P_s/P_p and the primary-jet pressure ratio P_p/p_0, corresponding to a boattail drag coefficient $C_{D,a}$, can be obtained from the base-to-free-stream static-pressure ratio p_b/p_0 and the use of figures 6 to 11.

Stream Effects on Jet Thrust for Typical Ejector Installations

The stream effects on ejector gross thrust for typical ejector installations utilizing a turbojet engine which delivers the following pressure ratios:

M_0	P_p/p_0
2.0	10
1.8	8
1.5	6

can readily be shown by comparing the ejector gross thrusts in quiescent air with those at supersonic speeds. The comparison of ejector gross jet thrusts indicate that quiescent-air data will overestimate the supersonic ejector gross jet thrust. The predicted errors for four configurations are shown in figure 15. It should be remembered that, since these results depend on the pressure ratio p_b/p_0, they are associated with the particular boattail configurations investigated.

For the ejector configurations shown (exclusive of configuration 1.70-0), the largest predicted errors are obtained at a free-stream Mach number of 1.5 at a primary-jet pressure ratio of 6. The largest error (17 percent) is obtained with ejector 1.70-0.56. As the diameter ratio is increased, the error in estimating ejector gross jet thrust increases. Likewise, increasing the spacing ratio from 0 to 0.56 (figs. 15(b) and (c), respectively) results in larger prediction errors at the supersonic Mach numbers investigated. However, a further increase in spacing ratio from 0.56 to 1.19 (figs. 15(c) and (d), respectively) decreases the prediction error. Increasing secondary weight flow also decreases the error, regardless of configuration.

SUMMARY OF RESULTS

An investigation was conducted in the Lewis 8- by 6-foot supersonic tunnel to determine external-stream effects on the gross thrust and pumping characteristics of several ejector-type exhaust nozzles operating at pressure ratios below design. Ejectors having diameter ratios of 1.16, 1.45, and 1.70 designed to operate at flight Mach numbers of 1.7, 2.2, and 2.6, respectively, were tested over a range of primary-jet pressure ratios and secondary weight flows at free-stream Mach numbers of 0, 0.63, 1.5, 1.8, and 2.0. The spacing ratio of the 1.70-diameter-ratio ejector was varied from 0 to 1.19.

The following results were obtained:

1. Adverse stream effects on ejector jet thrust resulted from low base pressures obtained at supersonic speeds.

2. The primary-jet pressure ratio above which the external-stream effects are eliminated decreased with decreasing diameter ratio and increasing spacing ratio.

3. Increases in secondary weight flow decreased the primary-jet pressure ratio above which quiescent- and supersonic-air data agree.

4. Mach number 0.63 and quiescent-air data agreed, regardless of configuration.

5. If a turbojet engine, delivering pressure ratios of 6, 8, and 10 at Mach numbers of 1.5, 1.8, and 2.0, respectively, is used in conjunction with the particular afterbody configurations investigated, quiescent-air data will overestimate the gross-jet-thrust ratio of high-diameter-ratio ejectors operating with low values of secondary weight flow. Gross-thrust-ratio prediction errors as high as 17 percent were obtained with ejector 1.70-0.56 at zero secondary weight flow. The largest errors in predicting gross thrust were obtained at a Mach number of 1.5 and a primary-jet pressure ratio of 6.

Lewis Flight Propulsion Laboratory
National Advisory Committee for Aeronautics
Cleveland, Ohio, March 19, 1956

REFERENCES

1. Hearth, Donald P., and Valerino, Alfred S.: Thrust and Pumping Characteristics of a Series of Ejector-Type Exhaust Nozzles at Subsonic and Supersonic Flight Speeds. NACA RM E54H19, 1954.

2. Stitt, Leonard E., and Valerino, Alfred S.: Effect of Free-Stream Mach Number on Gross-Force and Pumping Characteristics of Several Ejectors. NACA RM E54K23a, 1955.

3. Hearth, Donald P., and Gorton, Gerald C.: Investigation of Thrust and Drag Characteristics of a Plug-Type Exhaust Nozzle. NACA RM E53L16, 1954.

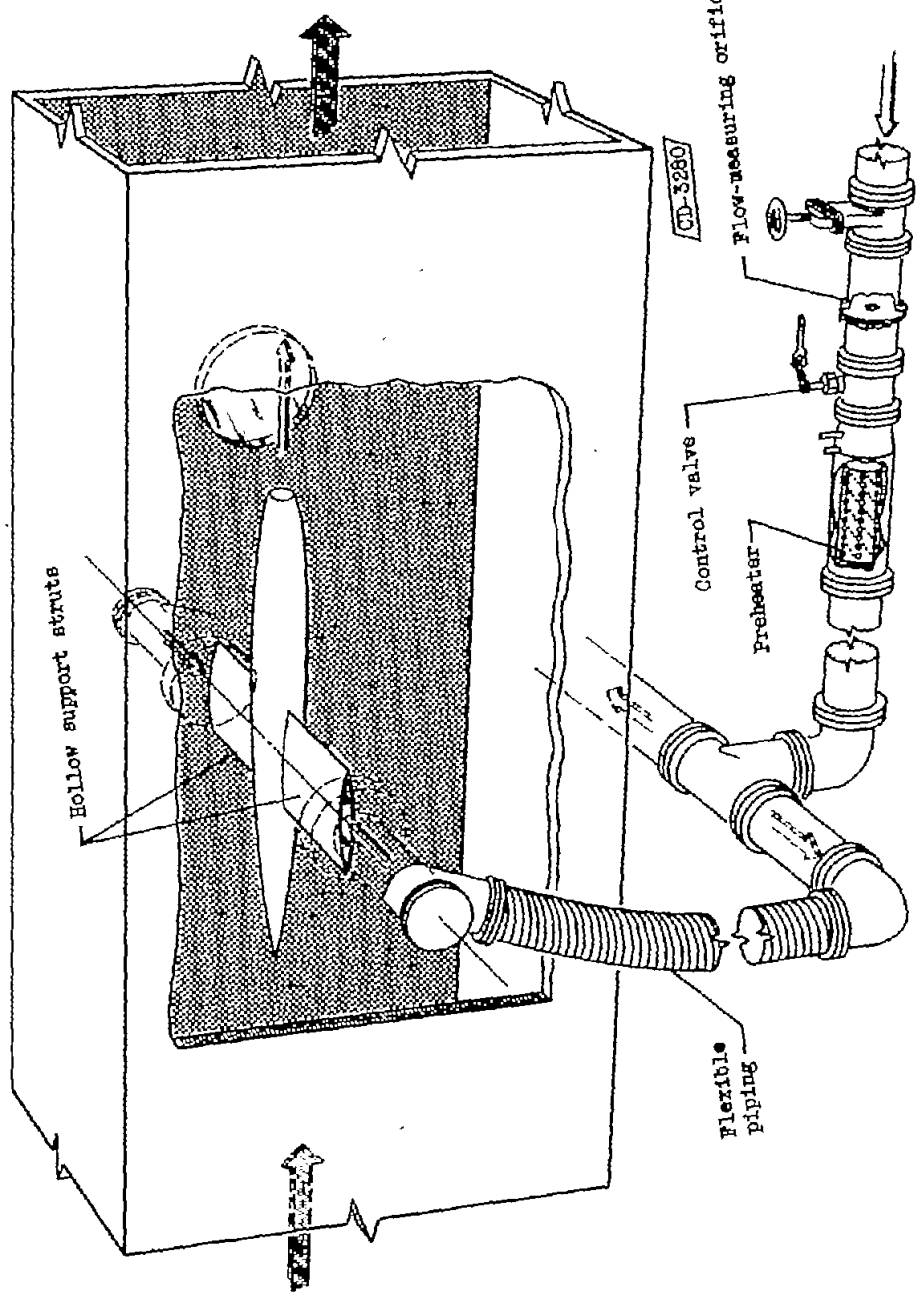

Figure 1. - Schematic drawing of jet exit model installed in 8- by 6-foot supersonic tunnel.

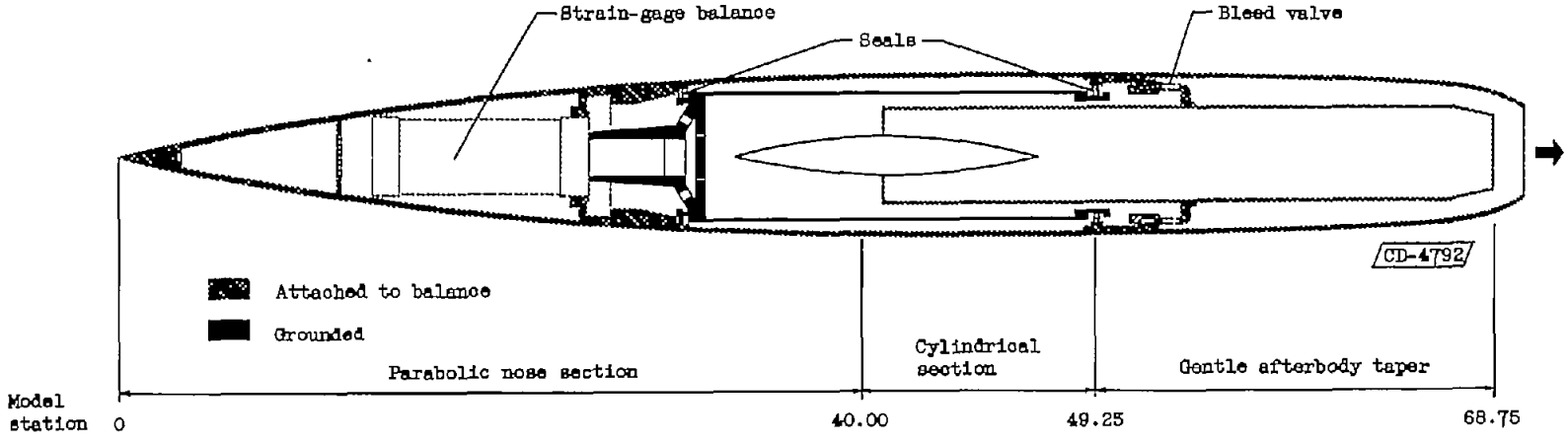

Figure 2. - Schematic diagram of jet exit model. (All dimensions in inches.)

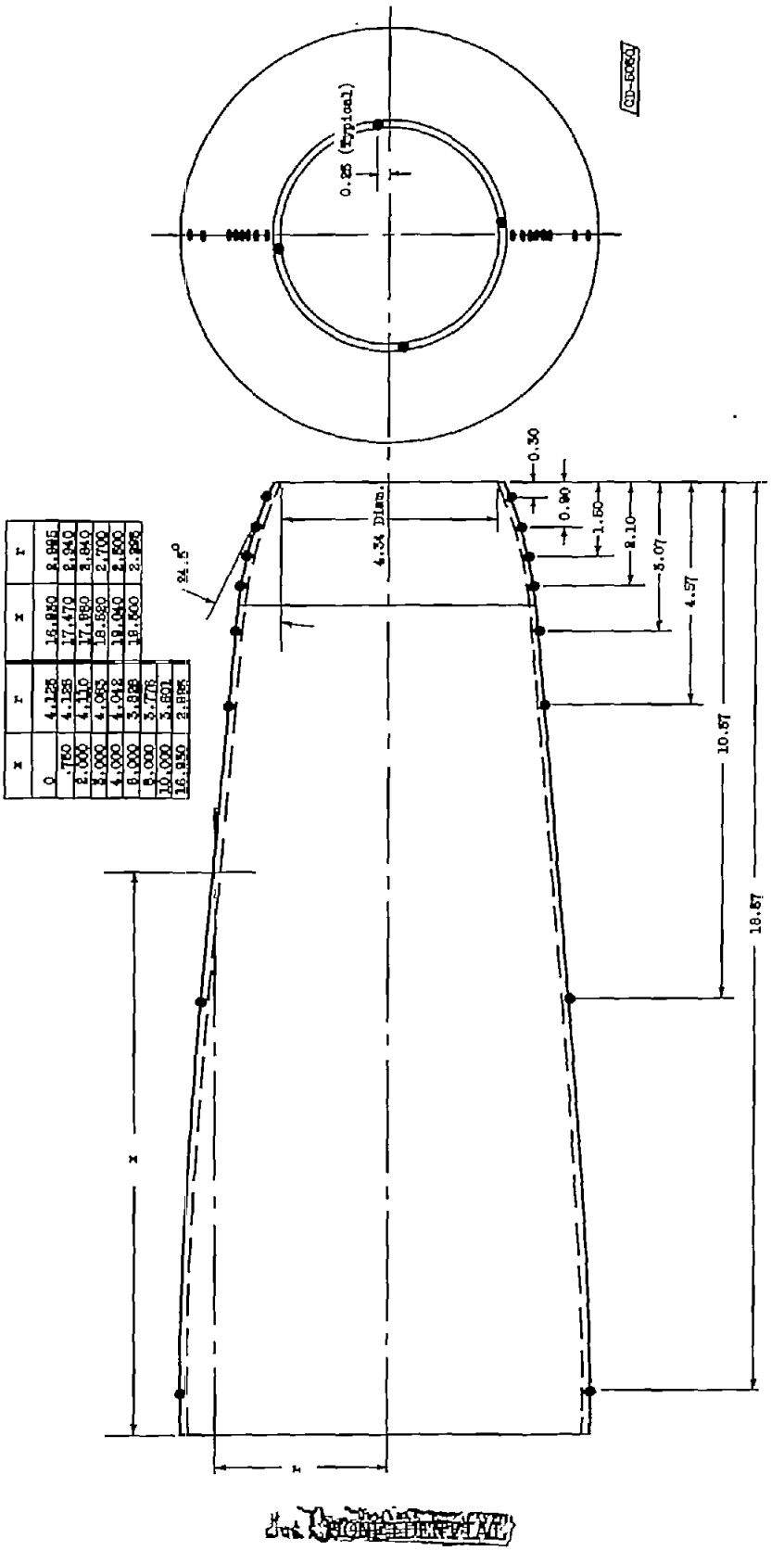

x	r
0	4.125
.760	4.125
2.000	4.110
3.000	4.063
4.000	4.042
5.000	3.828
8.000	3.776
10.000	3.601
16.930	2.895

x	r
16.930	2.895
17.470	2.840
17.880	2.840
18.580	2.700
18.840	2.600
18.900	2.595

Figure 5. - Coordinates of model afterbody. (All dimensions in inches.)

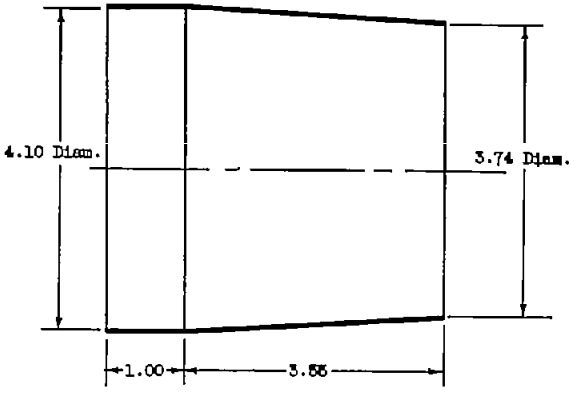

(a) Conical nozzle A.

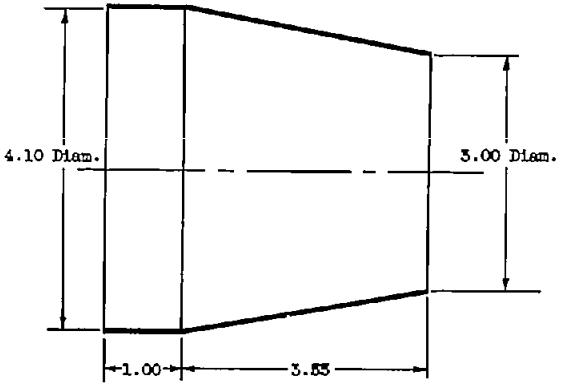

(b) Conical nozzle B.

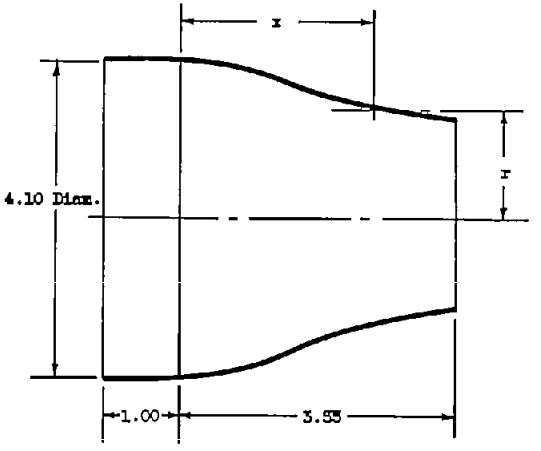

Coordinates of nozzle C	
x	r
0	2.050
.50	2.000
1.00	1.933
1.50	1.722
2.00	1.547
2.50	1.402
3.00	1.310
3.50	1.275

CD-5049

(c) Contoured nozzle C.

Figure 4. - Schematic diagrams of primary-jet exhaust nozzles. (All dimensions in inches.)

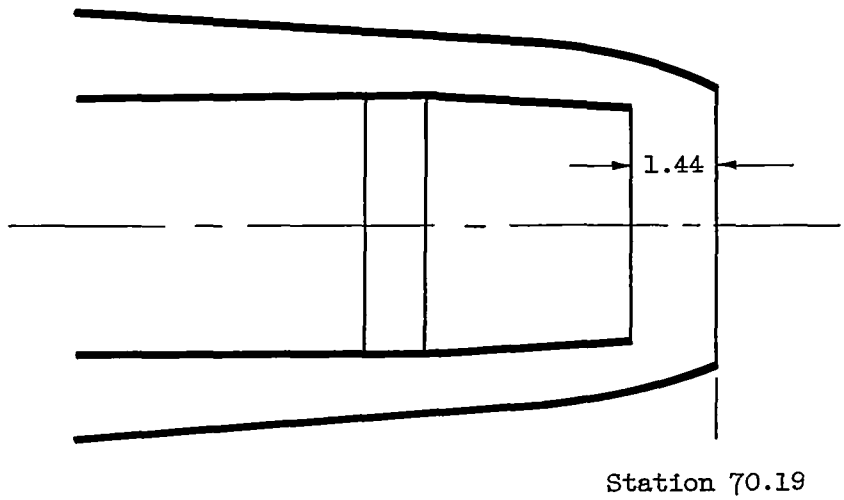

(a) Ejector 1.16-0.38.

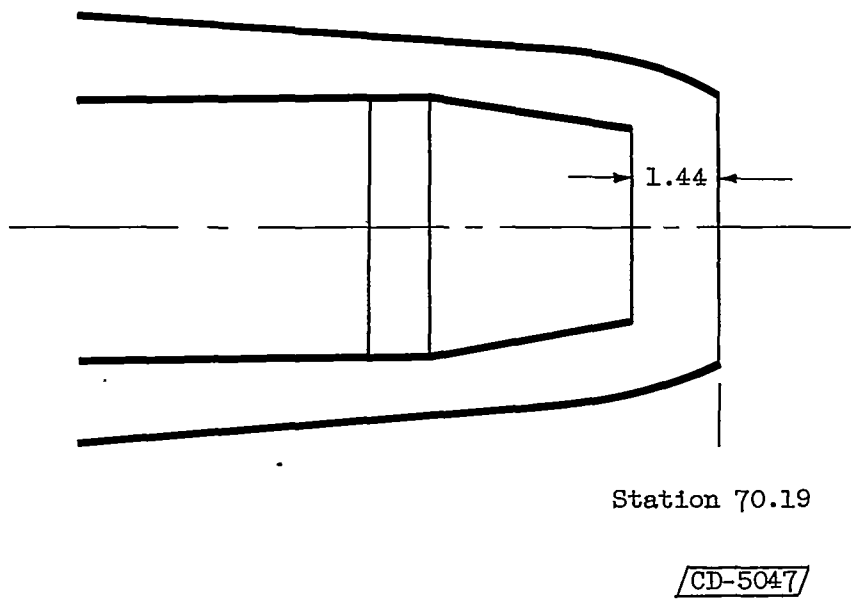

(b) Ejector 1.45-0.48.

Figure 5. - Ejector configurations. (All dimensions in inches.)

4026

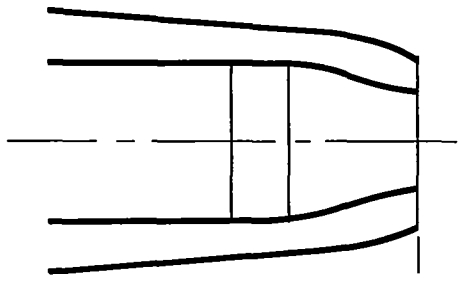

Station 68.75

(c) Ejector 1.70-0.

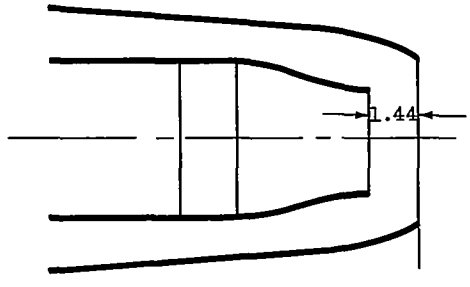

Station 70.19

(d) Ejector 1.70-0.56.

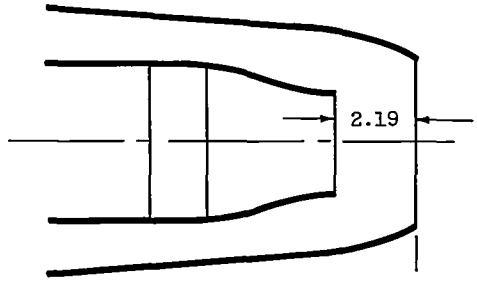

Station 70.94

(e) Ejector 1.70-0.85.

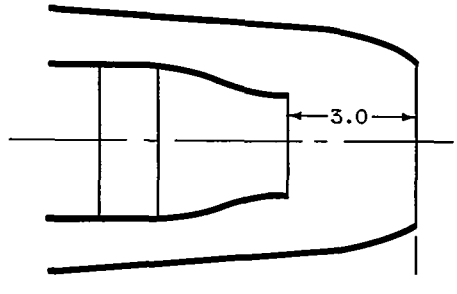

Station 71.75

(f) Ejector 1.70-1.19. CD-5048

Figure 5. - Concluded. Ejector configurations.
(All dimensions in inches.)

[redacted]

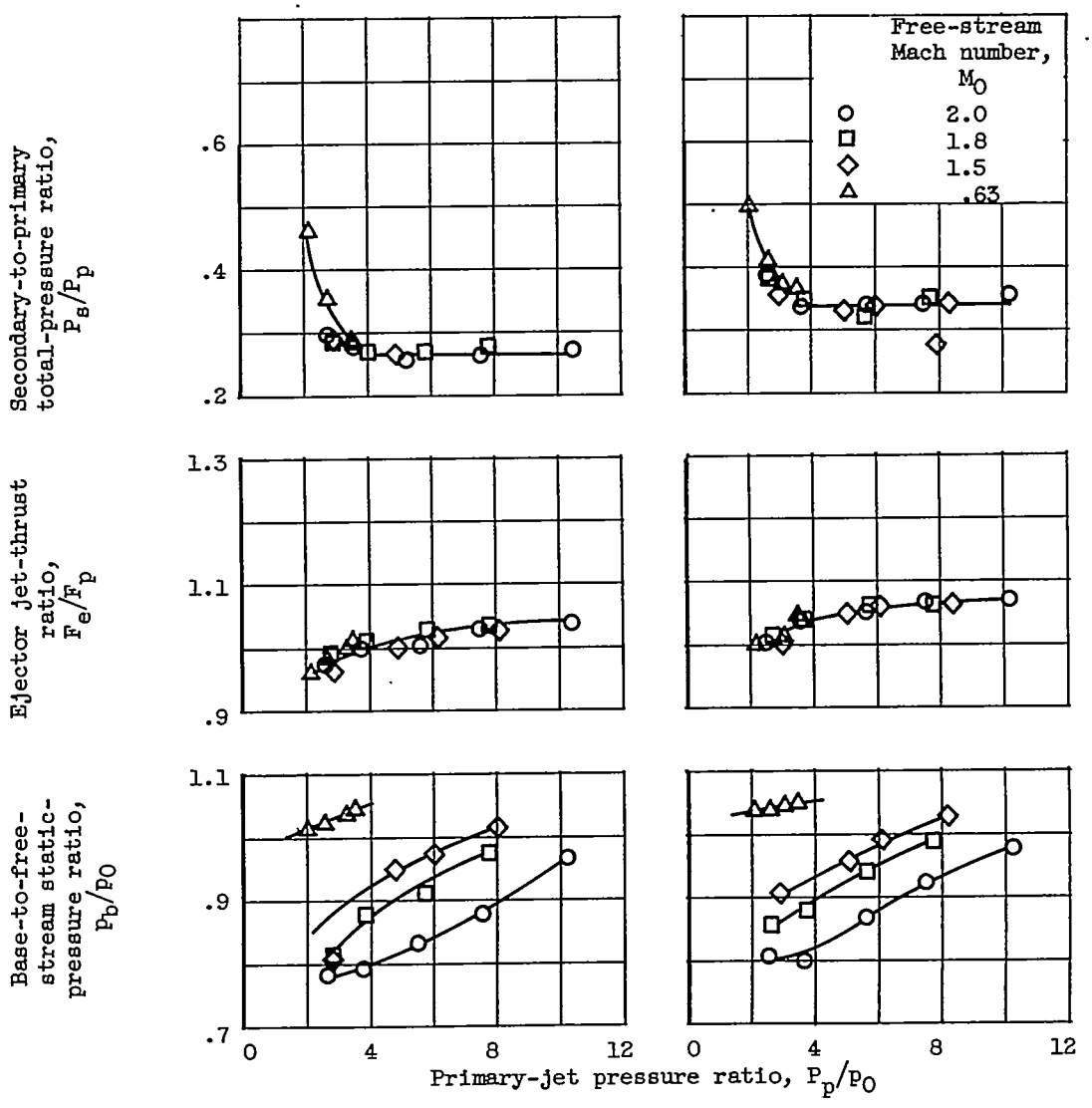

(a) Corrected weight-flow ratio, 0.

(b) Corrected weight-flow ratio, 0.05.

Figure 6. - Pumping, thrust, and base pressure characteristics of ejector 1.16-0.38.

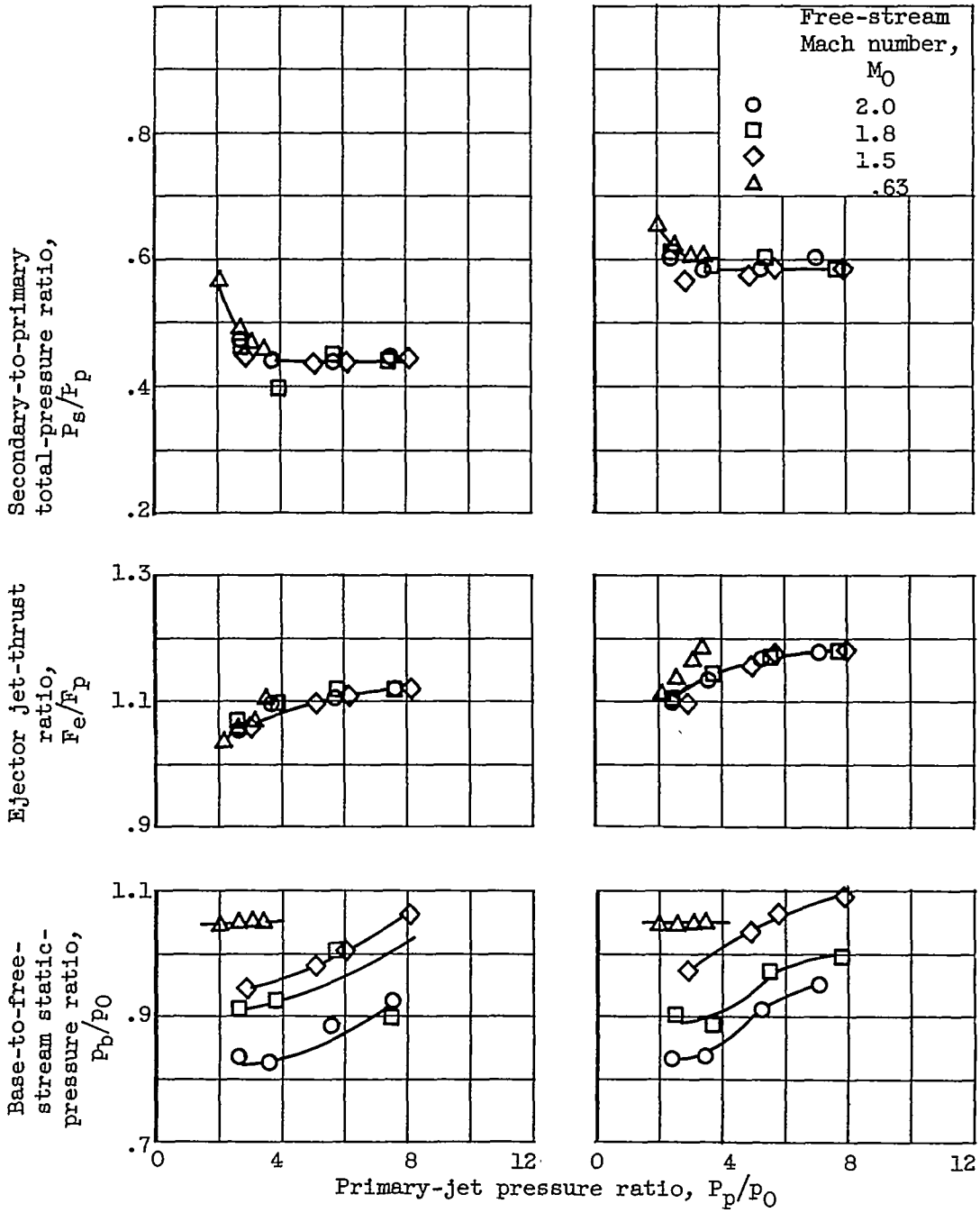

(c) Corrected weight-flow ratio, 0.10.

(d) Corrected weight-flow ratio, 0.18.

Figure 6. - Concluded. Pumping, thrust, and base pressure characteristics of ejector 1.16-0.38.

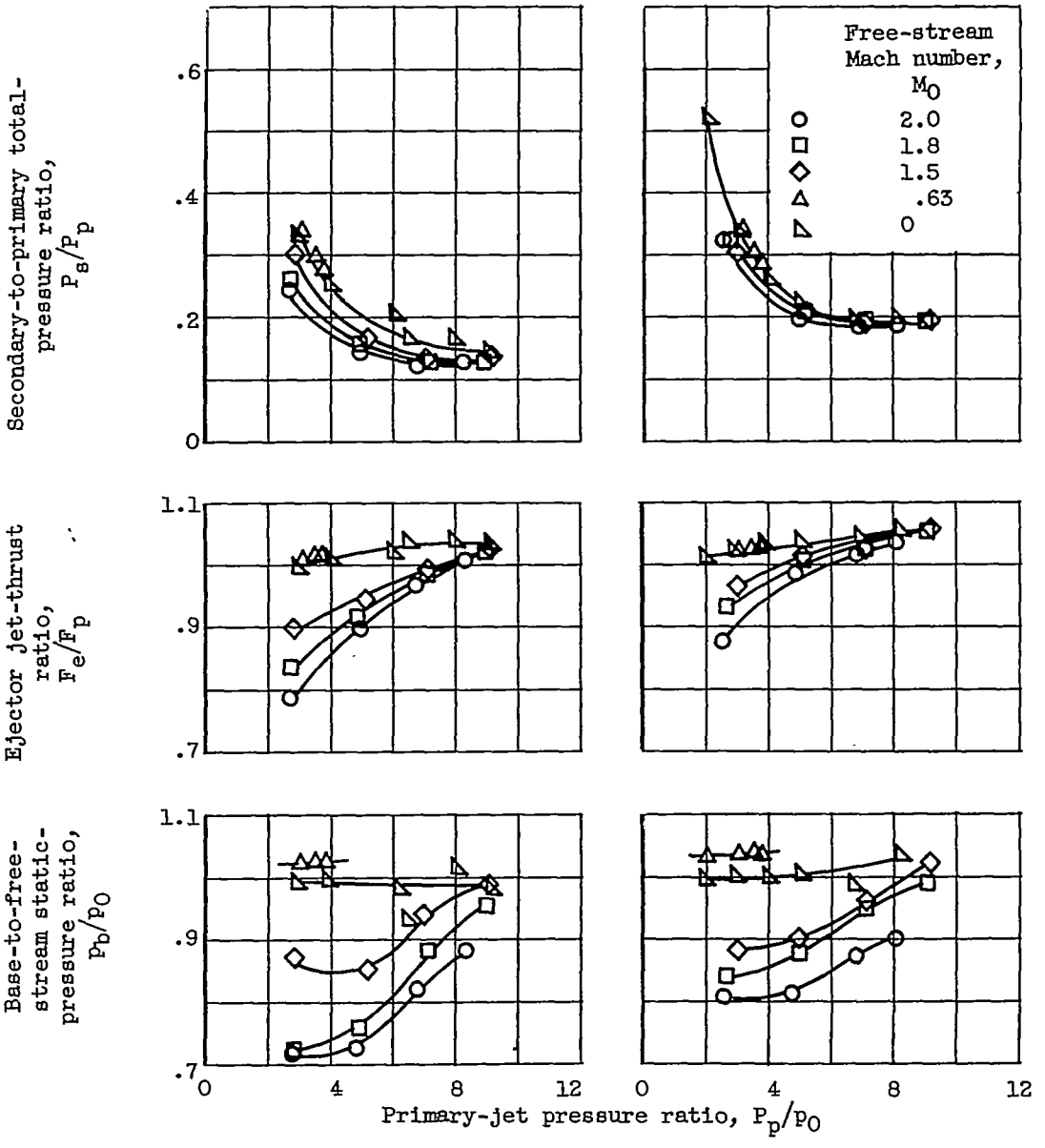

(a) Corrected weight-flow ratio, 0.

(b) Corrected weight-flow ratio, 0.06.

Figure 7. - Pumping, thrust, and base pressure characteristics of ejector 1.45-0.48.

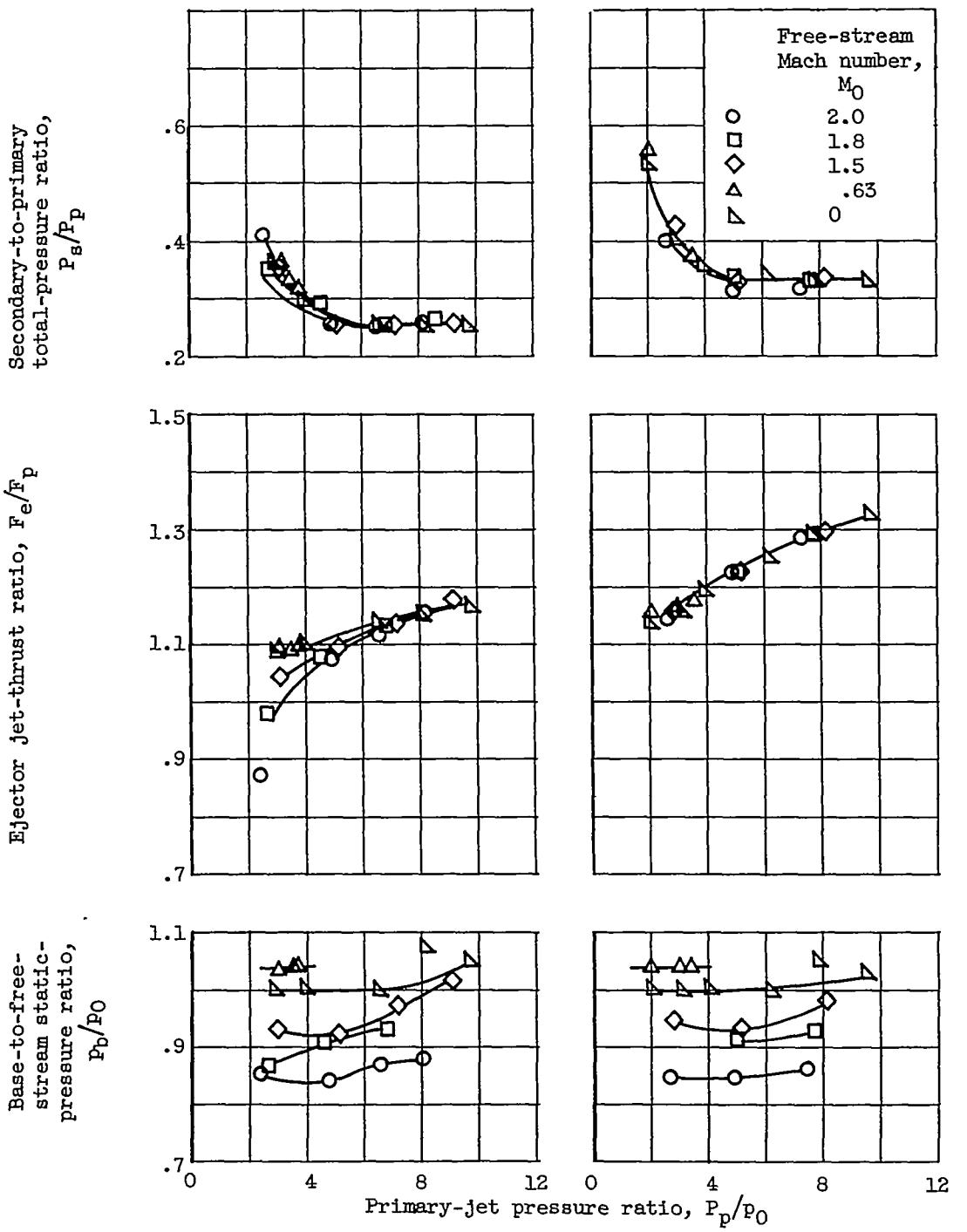

(c) Corrected weight-flow ratio, 0.15.

(d) Corrected weight-flow ratio, 0.24.

Figure 7. - Concluded. Pumping, thrust, and base pressure characteristics of ejector 1.45-0.48.

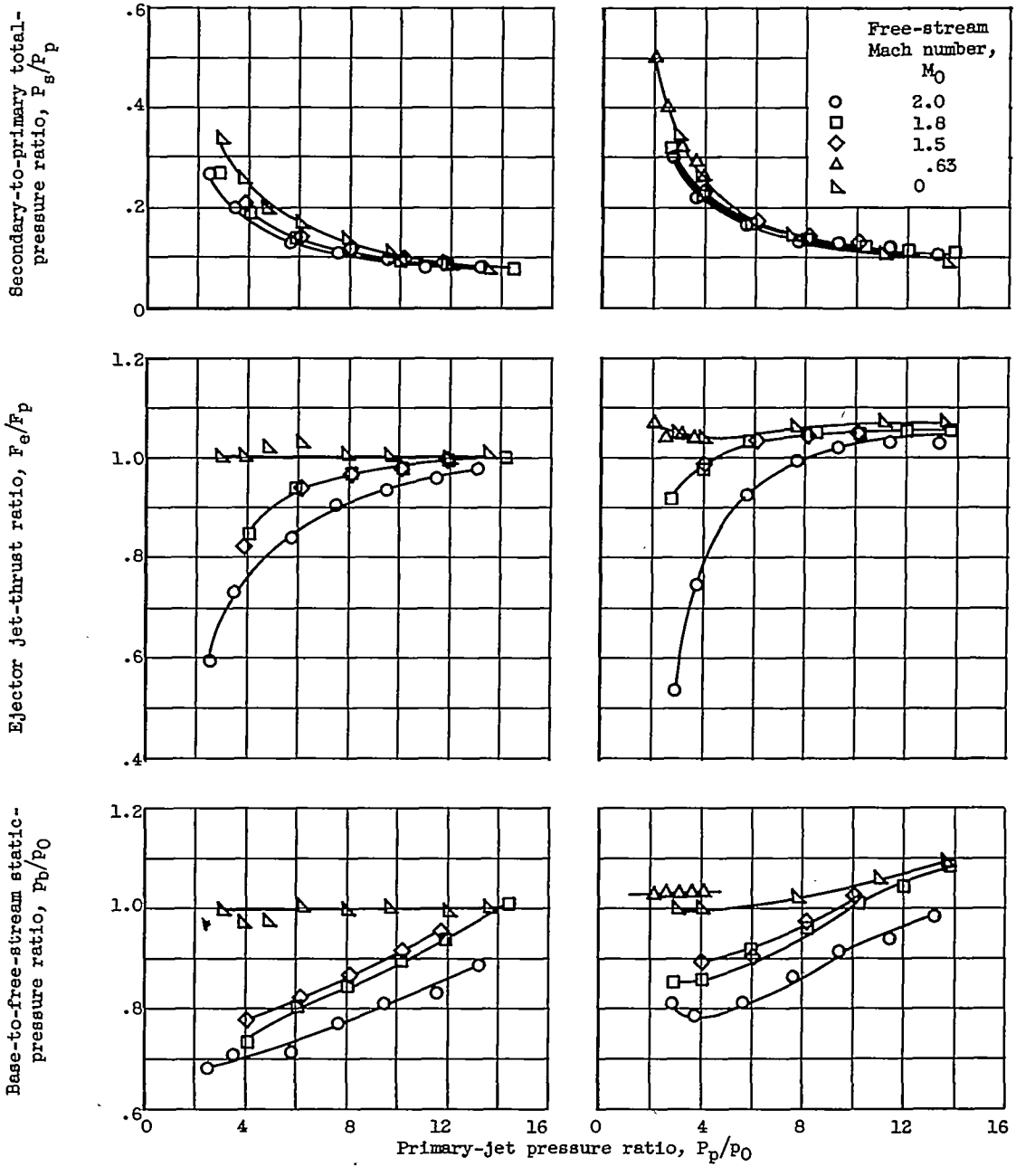

(a) Corrected weight-flow ratio, 0. (b) Corrected weight-flow ratio, 0.09.

Figure 8. - Pumping, thrust, and base pressure characteristics of ejector 1.70-0.

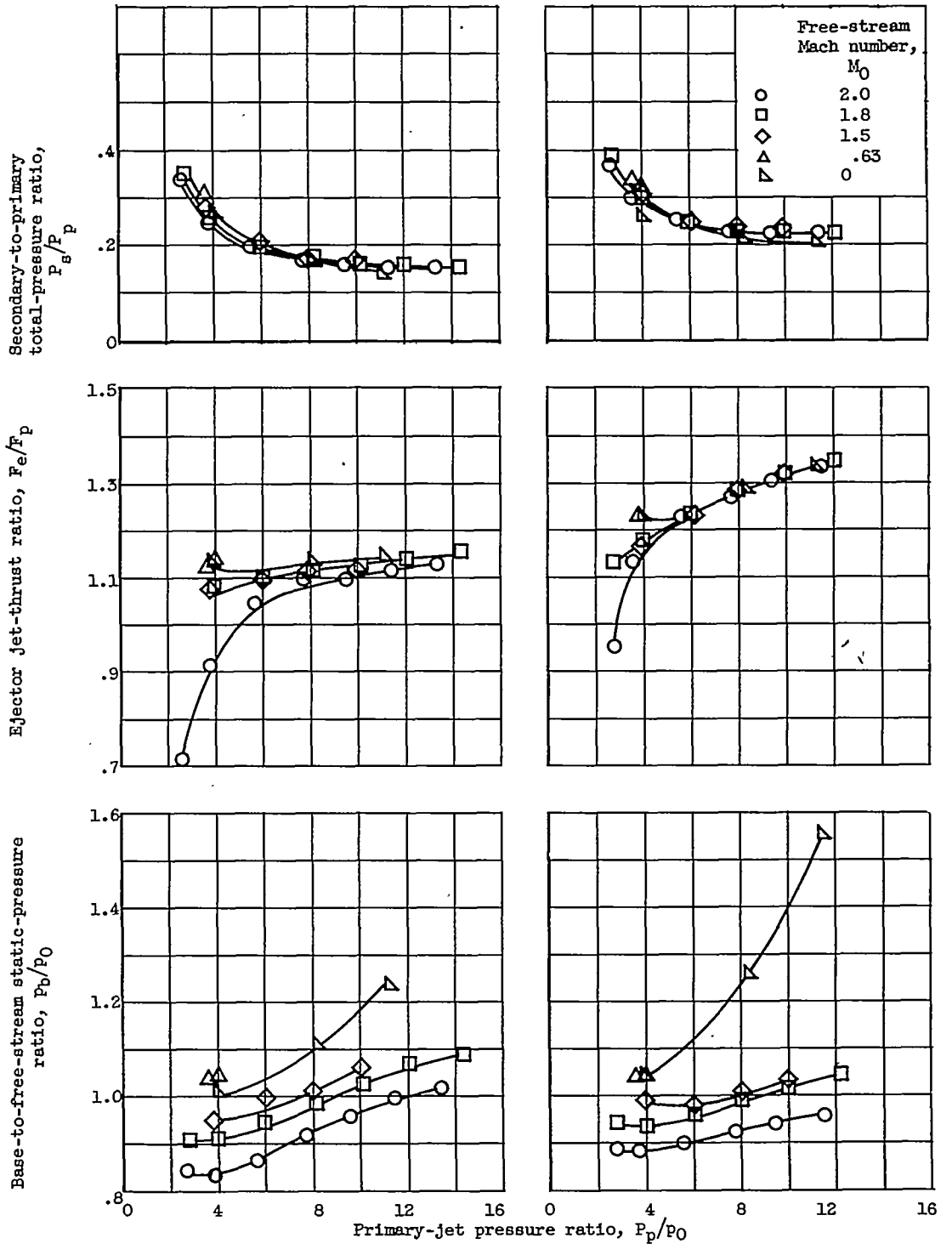

(c) Corrected weight-flow ratio, 0.19. (d) Corrected weight-flow ratio, 0.33.

Figure 8. - Concluded. Pumping, thrust, and base pressure characteristics of ejector 1.70-0.

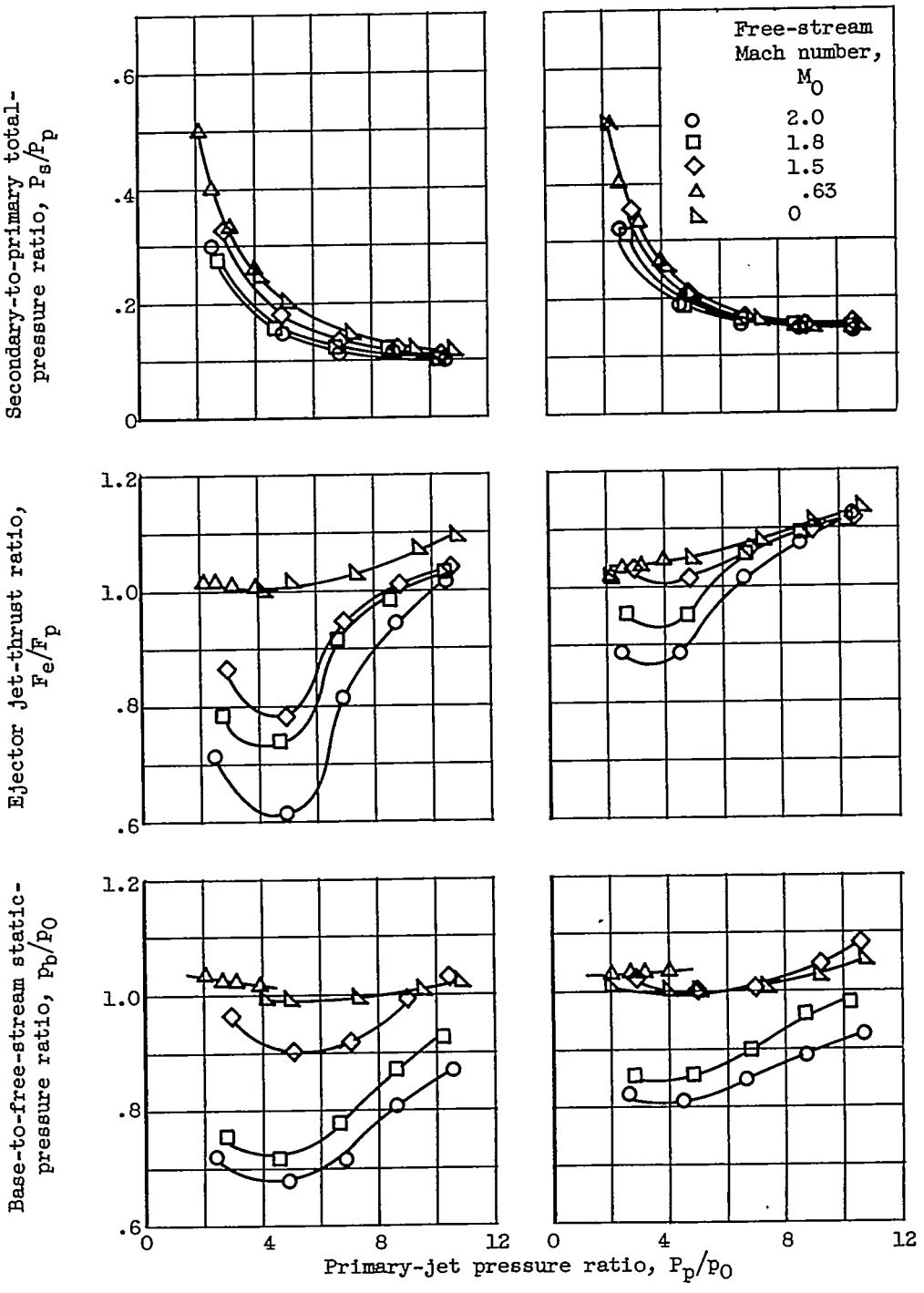

(a) Corrected weight-flow ratio, 0.

(b) Corrected weight-flow ratio, 0.09.

Figure 9. - Pumping, thrust, and base pressure characteristics of ejector 1.70-0.56.

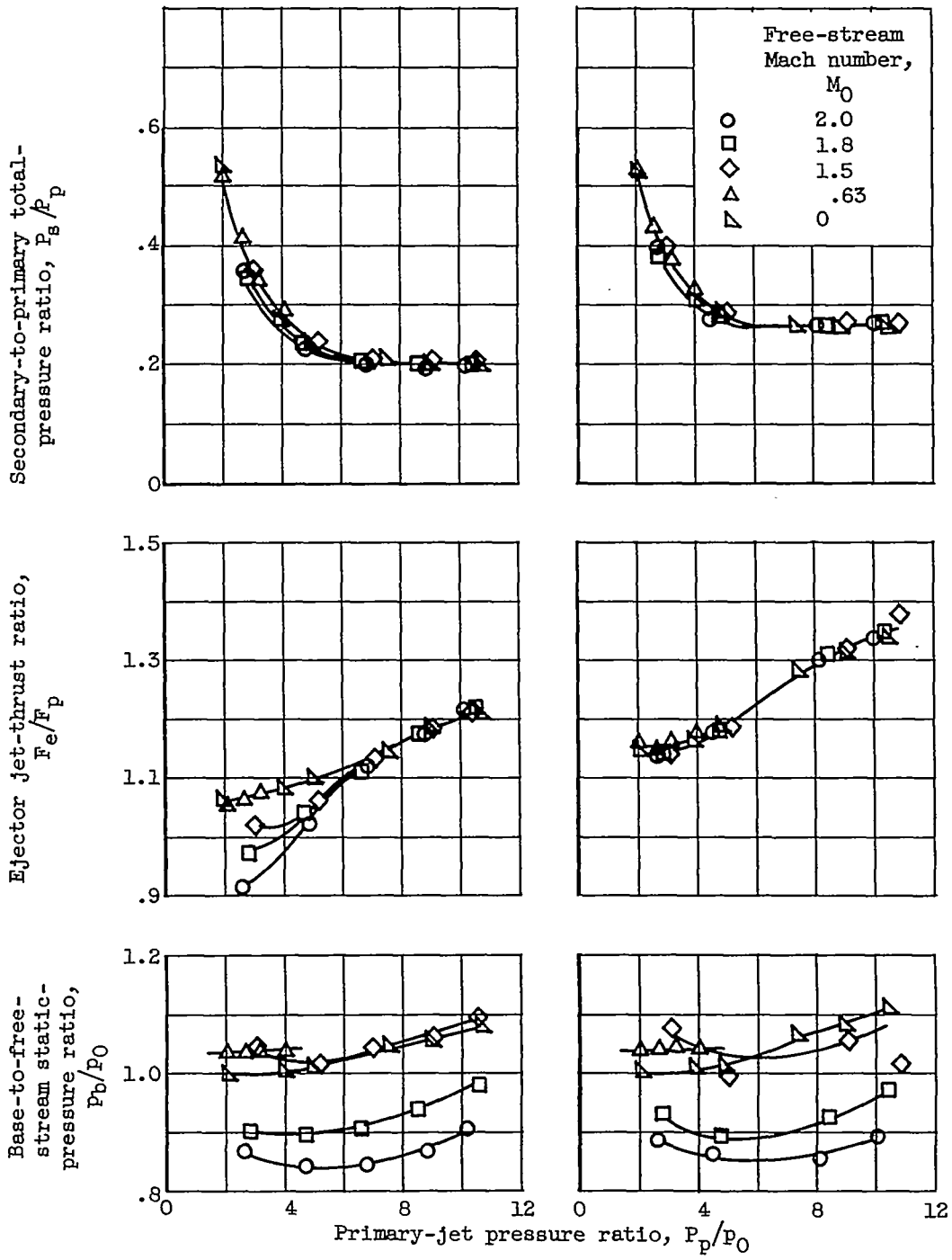

(c) Corrected weight-flow ratio, 0.19.

(d) Corrected weight-flow ratio, 0.33.

Figure 9. - Concluded. Pumping, thrust, and base pressure characteristics of ejector 1.70-0.56.

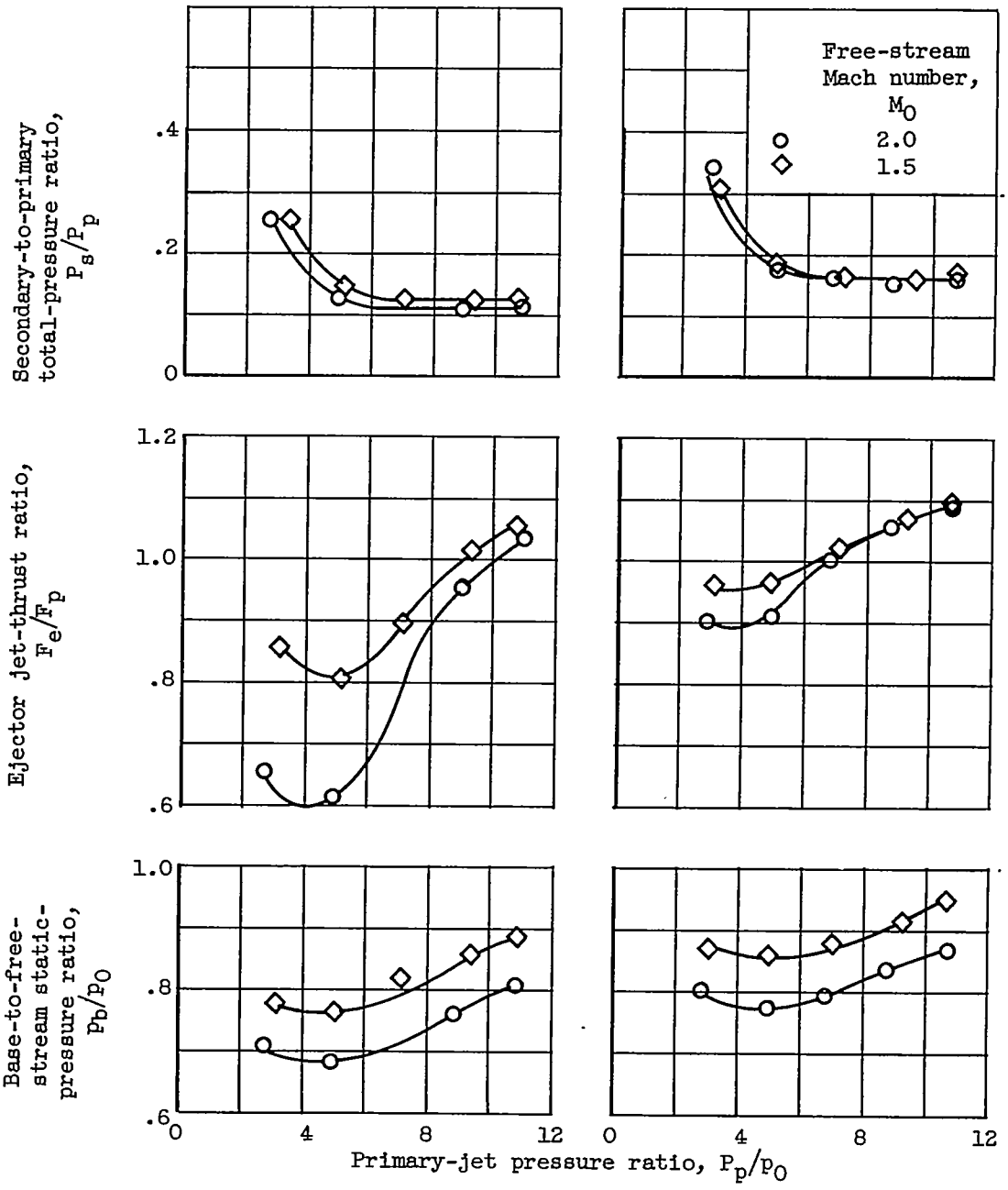

(a) Corrected weight-flow ratio, 0.

(b) Corrected weight-flow ratio, 0.09.

Figure 10. - Pumping, thrust, and base pressure characteristics of ejector 1.70-0.85.

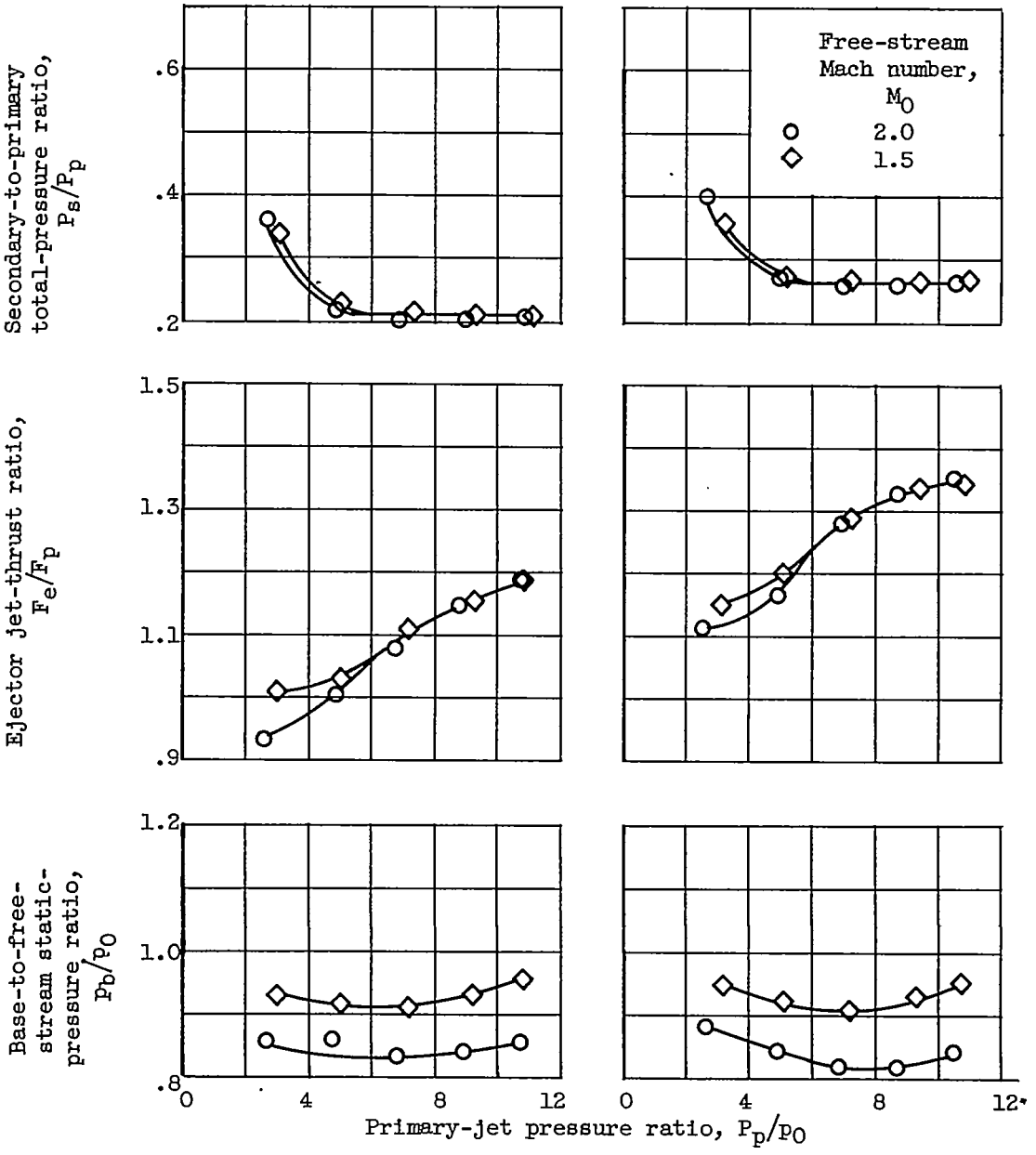

(c) Corrected weight-flow ratio, 0.19.

(d) Corrected weight-flow ratio, 0.33.

Figure 10. - Concluded. Pumping, thrust, and base pressure characteristics of ejector, 1.70-0.85.

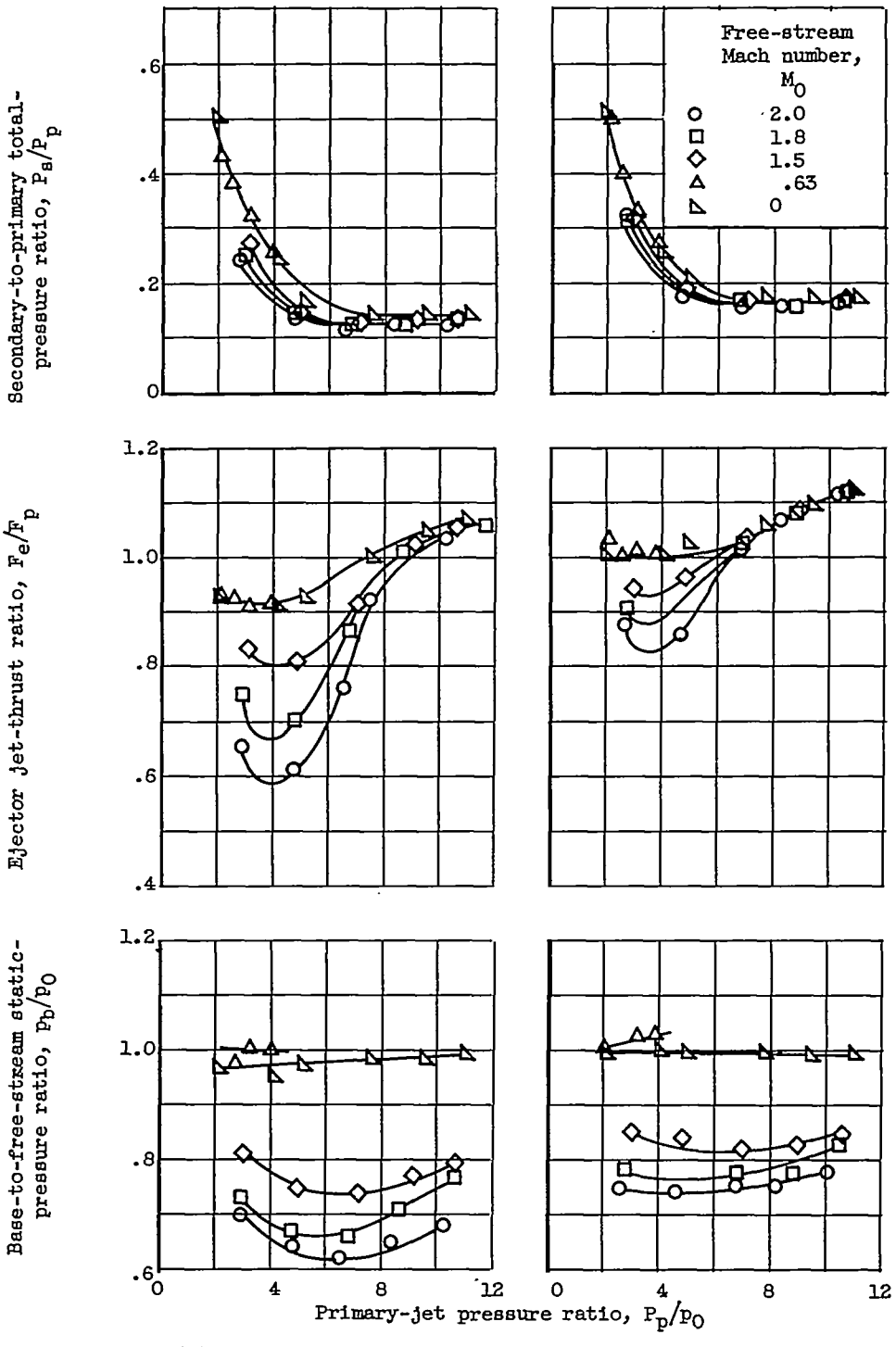

(a) Corrected weight-flow ratio, 0.

(b) Corrected weight-flow ratio, 0.09.

Figure 11. - Pumping, thrust, and base pressure characteristics of ejector 1.70-1.19.

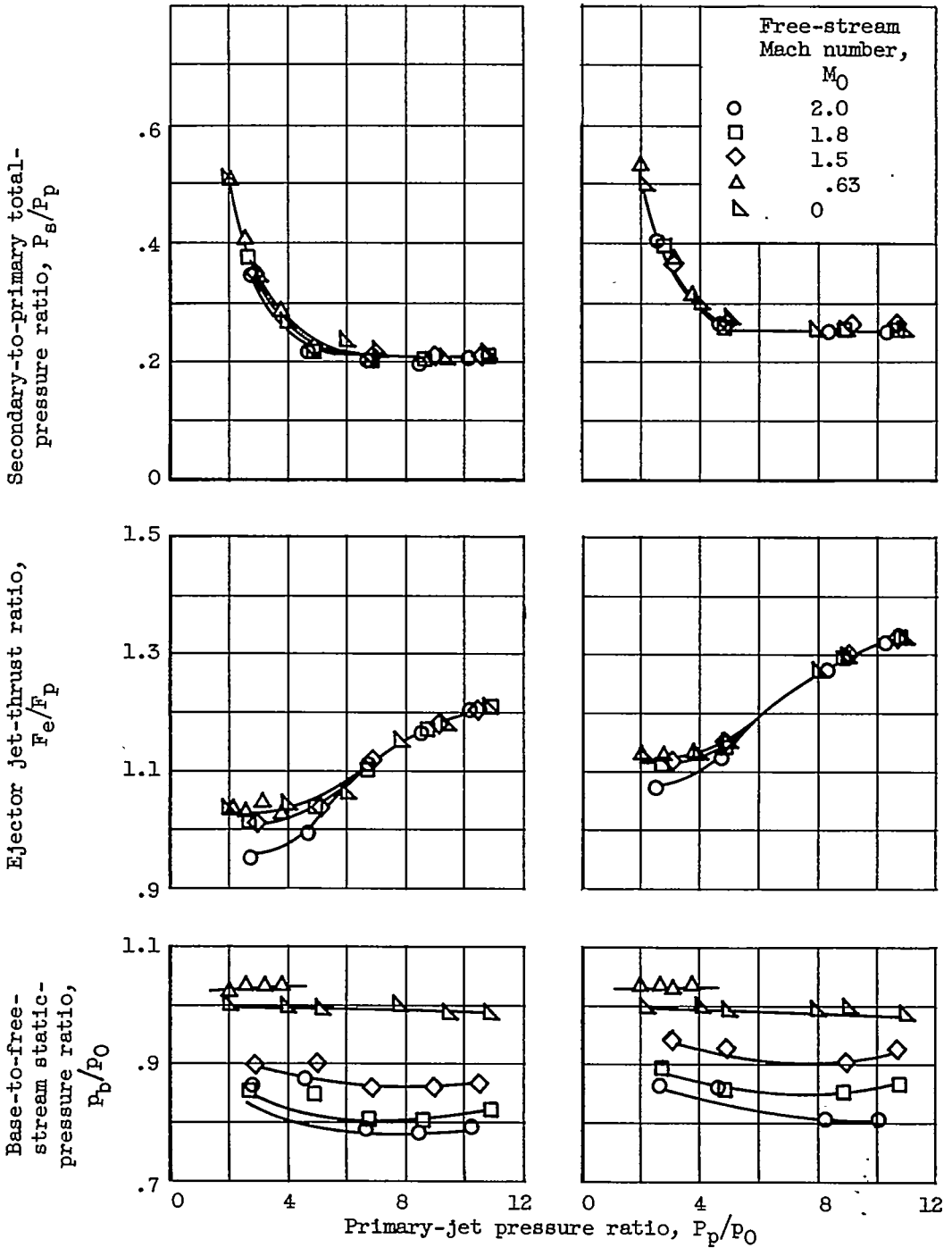

(c) Corrected weight-flow ratio, 0.19.

(d) Corrected weight-flow ratio, 0.33.

Figure 11. - Concluded. Pumping, thrust, and base pressure characteristics of ejector 1.70-1.19.

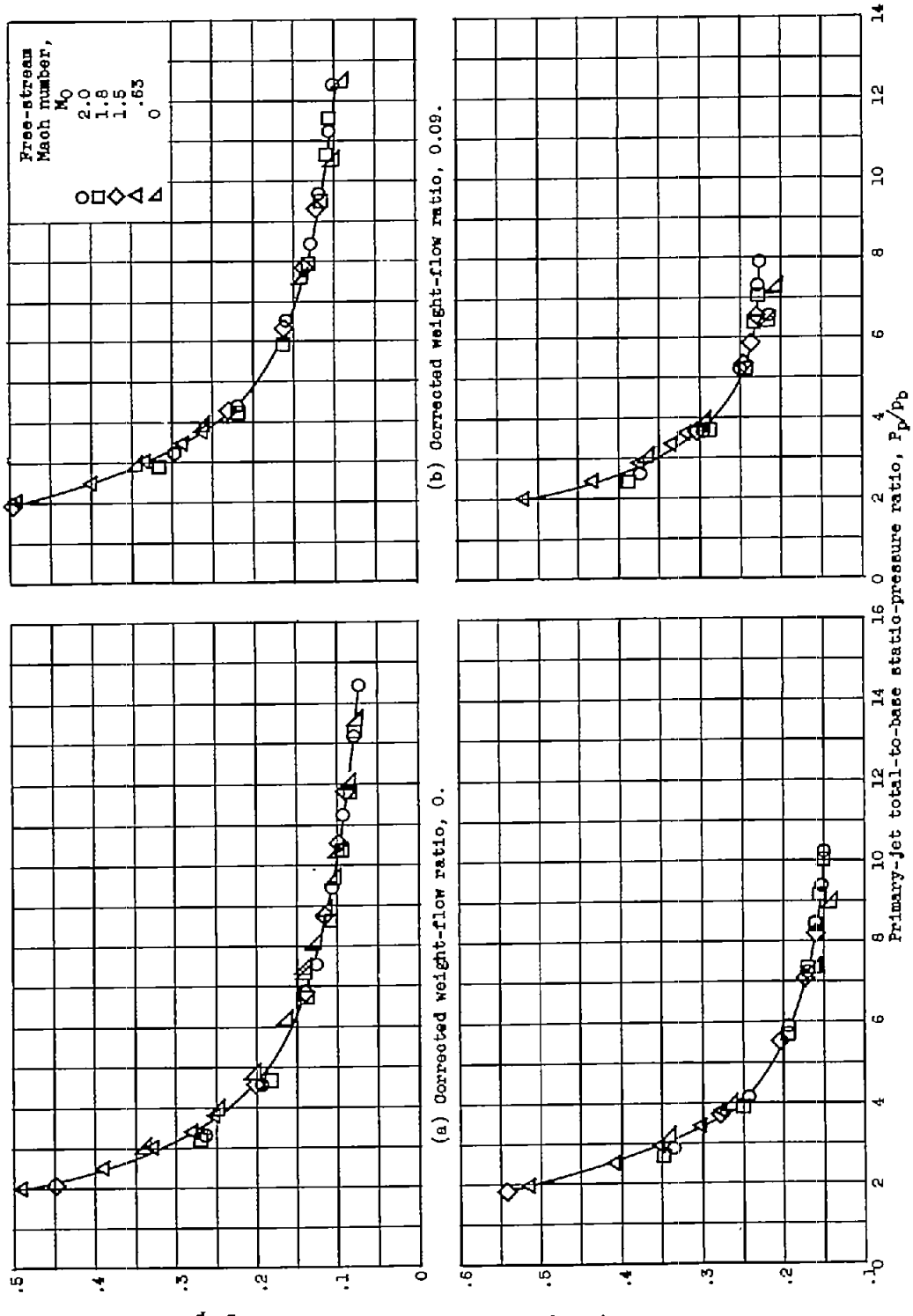

Figure 12. - Effect of base pressure on pumping characteristics.

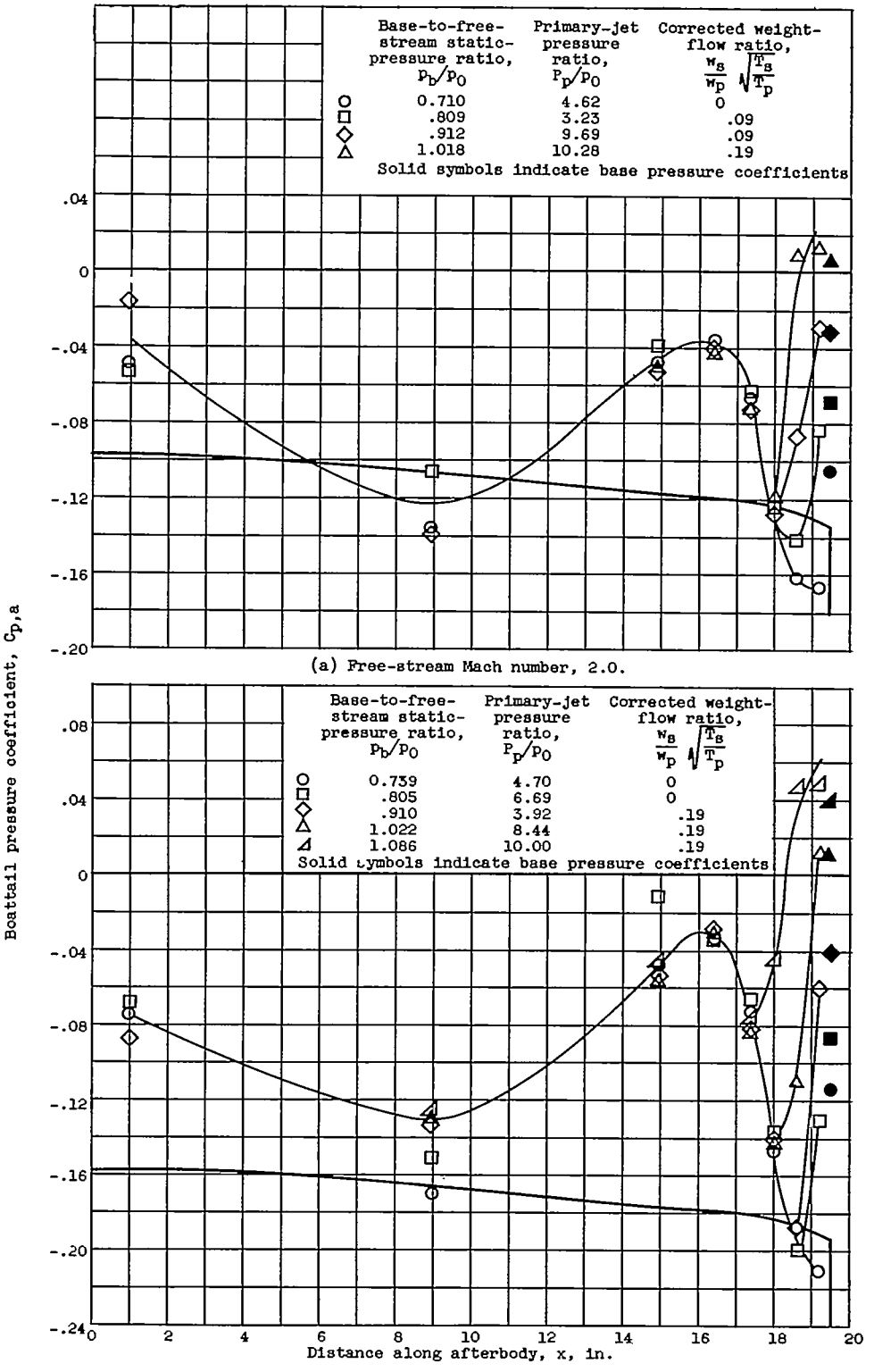

(a) Free-stream Mach number, 2.0.

(b) Free-stream Mach number, 1.8.

Figure 13. - Jet effects on afterbody pressures.

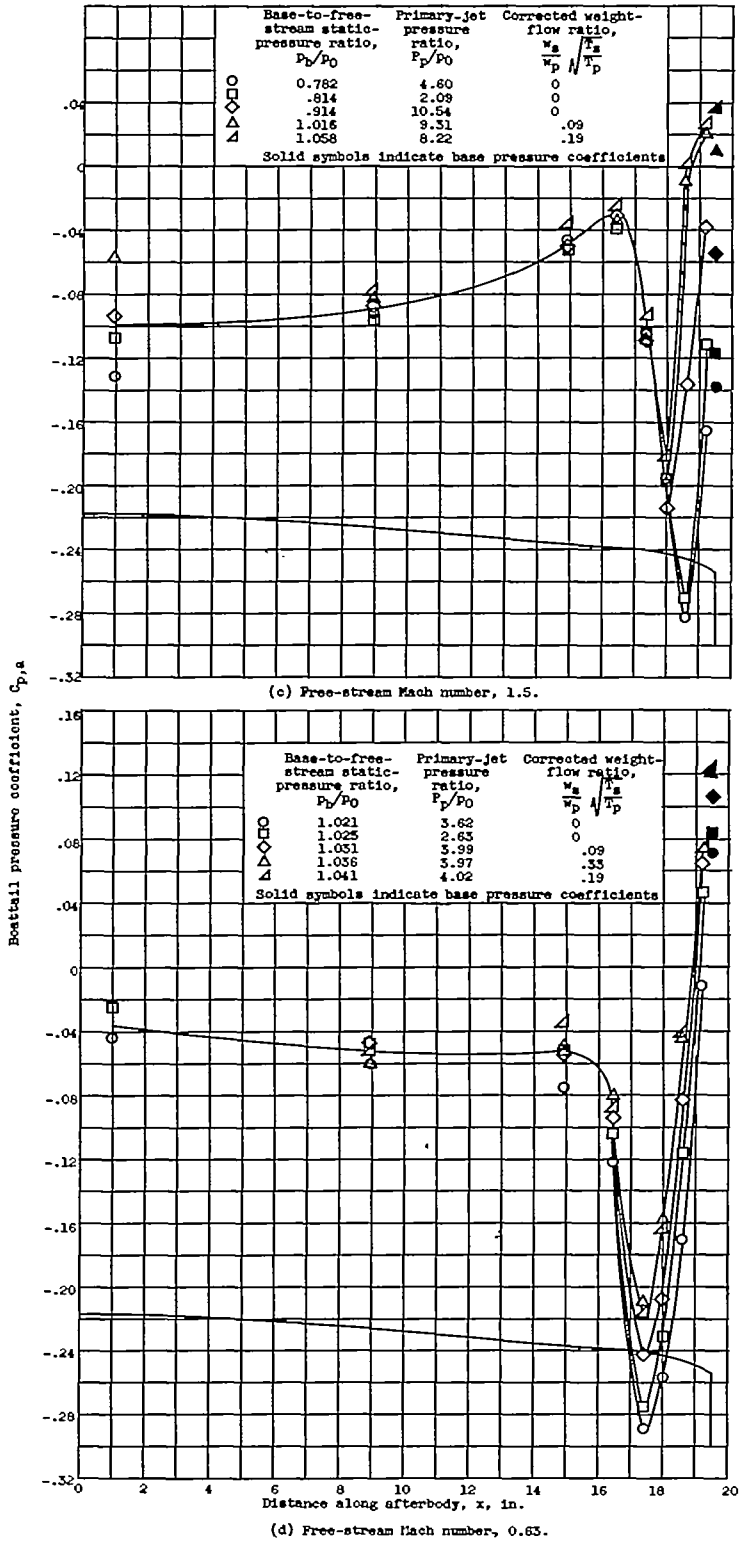

Figure 13. - Concluded. Jet effects on afterbody pressures.

4026

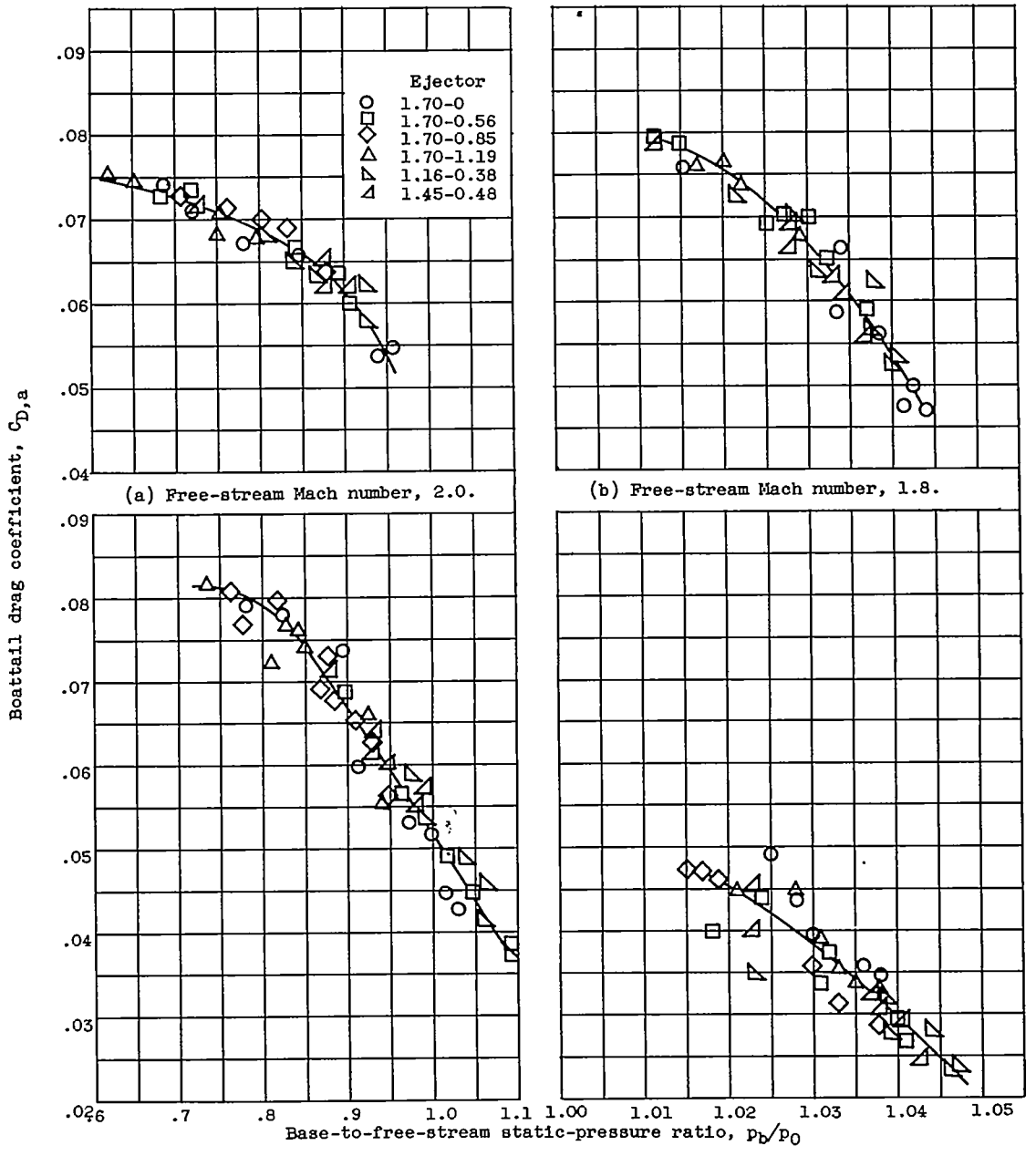

(a) Free-stream Mach number, 2.0.

(b) Free-stream Mach number, 1.8.

(c) Free-stream Mach number, 1.5.

(d) Free-stream Mach number, 0.63.

Figure 14. - Effect of base pressure on boattail drag coefficient.

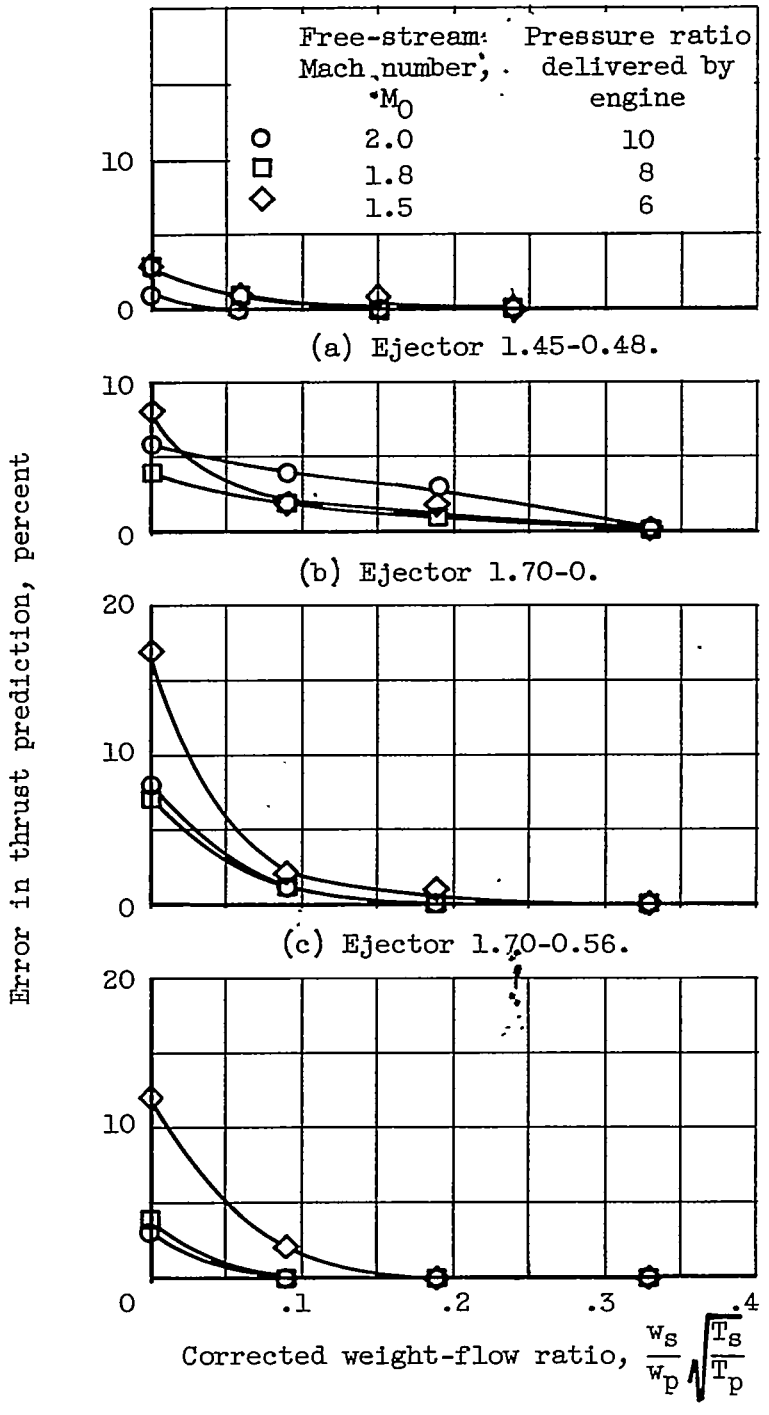

(a) Ejector 1.45-0.48.

(b) Ejector 1.70-0.

(c) Ejector 1.70-0.56.

(d) Ejector 1.70-1.19.

Figure 15. - Error in predicting ejector gross jet thrust from quiescent-air data.